# Heterogeneous cell performance of polymer electrolyte fuel cell at high current operation: Respiration mode as non-equilibrium phenomenon

*by* Ananda Putra

**Submission date:** 22-May-2023 03:46PM (UTC+0700)
**Submission ID:** 2099071737
**File name:** AIP_Advances_9-065206_2019_-artikel.pdf (14.68M)
**Word count:** 5916
**Character count:** 29701

AIP Advances ARTICLE scitation.org/journal/adv

# Heterogeneous cell performance of polymer electrolyte fuel cell at high current operation: Respiration mode as non-equilibrium phenomenon

Cite as: AIP Advances 9, 065206 (2019); doi: 10.1063/1.5099498
Submitted: 10 April 2019 • Accepted: 9 May 2019 •
Published Online: 12 June 2019

Satoshi Koizumi,[1,a)] Satoru Ueda,[1] Putra Ananda,[2] and Yasuyuki Tsutsumi[3]

## AFFILIATIONS

[1]Laboratory of Living Soft Matter, Institute of Quantum Beam Science, Ibaraki University 162-1, Shirakata, Ibaraki 319-1106, Japan
[2]Department of Chemistry, Faculty of Mathematics and Natural Science, Universitas Negeri Padang, Indonesia, 25131
[3]FC Development, Co., Ltd., Ibaraki University, 4-12-1 Nakanarusawa, Hitachi, Ibaraki 316-8511, Japan

[a)]To whom correspondence should be addressed. E-mail: satoshi.koizumi.prof@vc.ibaraki.ac.jp

## ABSTRACT

The heterogeneous performance of polymer electrolyte fuel cell in space and time was discussed for operation at high current density. The cell voltage, detected by a segmented electrode, varies along a gas flow channel from upper to bottom stream and oscillates in time, which is referred as a ***respiration*** mode. At the higher current, the cell voltage at different positions started to be synchronized, as the current density increases. In order to investigate a role of water on the respiration, we employed a new method of contrast variation for small-angle neutron scattering (SANS) using deuterium ($D_2$) gas as a fuel. By using $D_2$, we introduce special scattering contrast in a polymer electrolyte film (Nafion®), when the film is originally swollen by $H_2O$. After switching from $H_2$ to $D_2$ gas (humidified with $H_2O$), we found that SANS intensity significantly decreases about 40% at the $q$-position of scattering maximum ($q_m$) originating from the water-microdomains in the polymer electrolyte. After quantitative analyses of the scattering intensity, it was elucidated that 20 wt% of the total water is occupied by $D_2O$ as a steady state. At around the average intensity, SANS intensity oscillates with a time interval ~100sec, which corresponds to the respiration mode found for voltage. The respiration behavior is considered as a non-linear & non-equilibrium phenomenon in an open system, where water flooding plays a role of feedback to decelerate fuel transportation and chemical reaction of water generation.



## I. INTRODUCTION

A polymer electrolyte fuel cell (PEFC) is a sustainable and functioning system continuing power generation with moderate burn of hydrogen and oxygen gas. PEFC is considered as a model of living things to address a question what a living thing is. In PEFC, soft matters, i.e., a polymer electrolyte membrane (PEM) or membrane electrode assembly (MEA), is a key component to selectively transport protons between electrodes. Protons, separated from $H_2$ at anode catalyst, diffuse across MEA and reach to a reaction site of Pt surface at the cathode. According to chemical reactions, as follows

$$H_2 \rightarrow 2H^+ + 2e^- \quad \text{(Anode)},$$

$$2e^- + 2H^+ + 1/2\ O_2 \rightarrow H_2O \quad \text{(Cathode)},$$

we obtain the cell voltage $V_c$ =1.24 V, which is theoretically determined by Gibbs free energy difference $\Delta G_0$=228.6 kJ/mol.[1] A stack of cell components (gas diffusion layer (GDL), gas flow channel separators, clumping plates) sandwichs MEA (Figure 1). PEM is a mere material. However, it plays a key role in a cell system to control proton conduction and to sustainably continue power generation. We remind us that similarity is in the energy production of a living cell according to Mitchell chemiosmotic theory;[2] the electro chemical

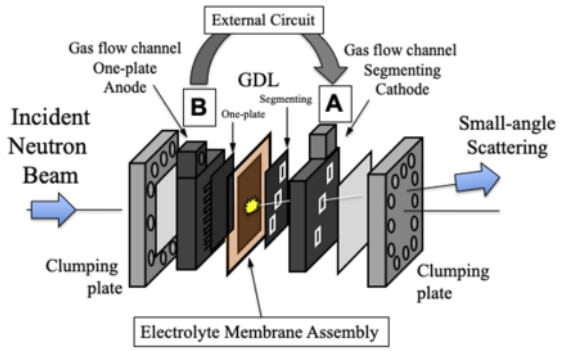


**FIG. 1**. Schematic diagram of polymer electrolyte fuel cell combined with small-angle neutron scattering and electric impedance methods (A and B denoted anode and cathode). Gas flow channel (electrode separator) and gas diffusion layer (GDL) at cathode are segmented into 3 sections, in order to examine the local cell performance.

gradient of proton across the membrane inside a microorganism (mitochondria) is a driving force for the bio-synthesis or active transport. Using the energy, a membrane protein, Atphase, synthesizes adenosine triphosphate (ATP) from adenosine diphosphate (ADP) and inorganic phosphates. We expect that PEFC during operation, an open system in a non-equilibrium & steady state, allow us to explore a boundary between materials and life.

In this paper, we report on heterogeneity in the power generation in space and in time occurring at high current operation. We found that cell voltage starts to oscillate with a time interval $\Delta t$ ~100 sec. We refer this phenomenon to a ***respiration*** mode. First, the respiration starts at different positions along a gas flow channel and not synchronized. Note that in our PEFC, a serpentine-shape gas flow channel traces a membrane surface. At a higher limit of current, corresponding to oxygen diffusion loss, the respiration at different positions starts to be synchronized in a plane direction. This non-equilibrium behavior is related to water flooding at a reaction site of cathode. Flooding plays a role as feedback mechanism decelerating mass transportation of oxygen gas and therefore water production.

In this study, small-angle neutron scattering (SANS), which is an essential method for materials science, plays a key role to observe membrane structure and water distribution ranging in nano-scales selectively in a cell stack. Due to the characteristics of no charge, neutron can easily pass through a PEFC with thickness of several centimeters. SANS quantitatively determines the structure of water-channels and its swelling degree by water, which strongly influences proton conductivity. In the previous publications,[3–6] flooding in a flow channel at the cathode, detected by neutron radiography (NR) and discussed in a relation with swelling (SANS) and resistance of the membrane, detected by using a segmented electrode. When the membrane is fully swollen with water, which was confirmed by SANS, flooding appears in the gas flow channel at the cathode, detected by NR.[3–5]

In this study, SANS was further reinforced by developing the deuterium fuel cell; we switched fuel gas (from $H_2$ to $D_2$) during operation, we introduce a change in a scattering contrast $\Delta b^2$ in a polymer electrolyte membrane (Nafion®212). Consequently, time-resolved SANS detects a rhythmic oscillation of SANS intensity at a wave number ($q$) corresponding to inter-distance of water cluster-network.[7] Scattering contrast, given by a mixing ratio $H_2O$ and $D_2O$ (or $D^+$ and $H^+$), oscillates in a course of operation (respiration mode). A local observation of cell performance (local resistance, voltage or current values) is done by a segmented electrode in order to complementary discuss the local information acquired by SANS and NR.

In addition, we report that PEFC using deuterium gas exhibits higher cell performance (5% in voltage) as compared to normal PEFC using $H_2$. This is due to difference in Gibbs free energy between $H_2$ and $D_2$. In order to investigate history of water related to the respiration, we employ a new method of contrast variation, i.e., deuterium gas polymer electrolyte fuel cell. We operate a polymer electrolyte fuel cell (PEFC) using deuterium ($D_2$) gas as a fuel (deuterium fuel cell), as well as hydrogen gas ($H_2$).

## II. EXPERIMENTAL

### A. Small-angle neutron scattering

We employed a SANS instrument (SANS-J-II), at research reactor JRR3 of Japan Atomic Energy Agency (JAEA), Tokai, Japan. SANS-J-II spectrometer, was originally constructed as a pin-hole type SANS instrument with a long scattering flight path (10m) and collimator chamber (10m), and recently reinforced by a focusing method using refractive or magnetic lens in order to reach to ultra-small scattering angle.[8] To detect water in an operating fuel cell over a wide length scale from nanometers to centimeters, a neutron imaging camera was installed at the sample position of SANS-J-II.[3] Monochromatic neutron of $\lambda$ = 6A was used with a size of 10 mm in diameter. The beam was irradiated at a center of fuel cell during operation. After subtracting the background scattering from cell components and incoherent scattering from hydrogen atoms, circular-averaging of 2-dimesional data was performed in order to obtain scattering profile as a function of $q$ (a magnitude of scattering vector, as defined $q = 4\pi/\lambda \sin(\theta/2)$ where $\lambda$ and $2\theta$ are wave length and scattering angle, respectively).

### B. Contrast variation method

#### 1. Water mixing ($H_2O/D_2O$)

To quantitatively evaluate SANS intensity, A Nafion®212 films (50 μm thickness) was swollen by mixed water ($H_2O/D_2O$) (conventional contrast variation). Mixed water ($H_2O/D_2O$) was variously prepared for every 10%. The film specimen was packed in a sample holder with aluminum thin windows and SANS measurements were performed by irradiation neutron beam through a film.

#### 2. Gas mixing ($H_2/D_2$)

To trace water (hydrogen) movement, we propose to use contrast variation with gas exchange ($H_2$ and $D_2$). We switched a fuel cell from $H_2$ to $D_2$ during operation. When we operate a fuel cell with $D_2$, deuteron ($D^+$) or deuterated water ($D_2O$), generated from $D_2$, swells a membrane in an operating fuel cell. Hydrogen gas ($H_2$ and $D_2$) is supplied by a electrolysis generator (Shimazu Co. Ltd.,

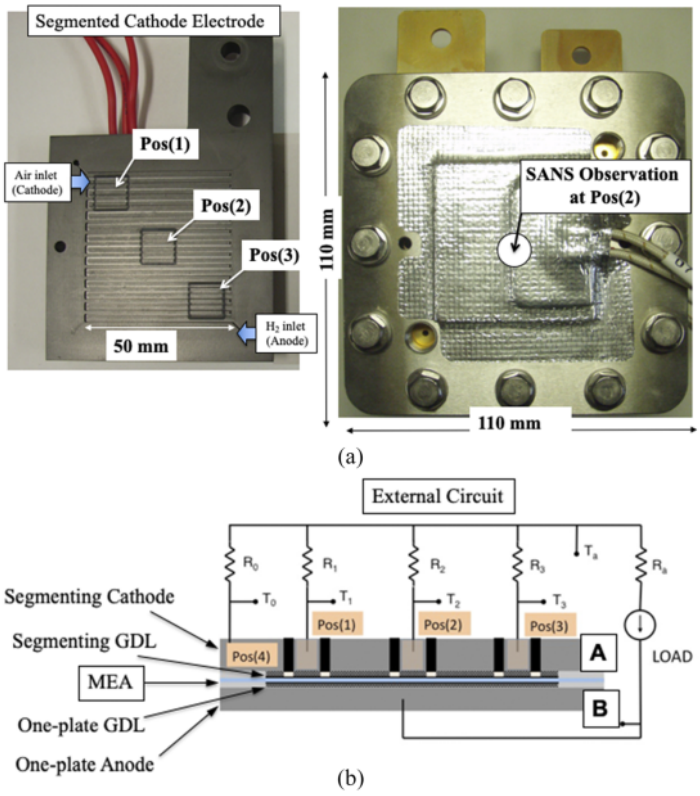


**FIG. 2**. (a) Photograph of segmented electrode separator (left) and a JARI standard cell (right). Segmented sections of gas flow channel designated are indicated as pos(1), (2) and (3). A JARI standard cell is modified in order to irradiate neutron at position pos(2) and perform SANS measurement. (b) Schematic diagram for electric circuit with segmented electrode sections, indicated by pos(1), (2), (3) and (4), respectively. $R_i$ and $T_i$ (i=0-1 or a) indicate shunt resistances and terminals. Parts A and B correspond to anode and cathode electrodes as shown in Figure 1.

Japan). Temperature, humidity and a flow rate of gas are controlled by an apparatus provided by FC Development, Co., Ltd., Hitachi Japan. An electronic load unit (PLZ164WA, Kikusui Electronics Corp.) was used for resistance load in order to operate PEFC. For in-situ SANS, temperature of the test cell was operated at 80 °C. The flow rate of anode and cathode gas ($D_2$ and air) was 200 and 800 SCCM. Temperature of the gas and bubbler filled with $H_2O$ was controlled at 80 °C.

### C. Test fuel cell

A single fuel cell (see Figure 2), originally developed by Japan Automobile Research Institute (JARI model), was modified for SANS and electric experiments. A gas flow plate, which was originally made of carbon/epoxy composite, was replaced with aluminum in order to minimize background for small-angle scattering. Using a gas flow channel of a serpentine shape (1mm depth and width), hydrogen and air are supplied from bottom and from the top (*counter-flow* condition). Temperature of the fuel cell is controlled by sheet heaters attached on the surface.

To observe local cell performance, i.e., cell voltage, a segmented separator was used.[5,6] To make them independent and isolated from the matrix, insulating epoxy resin was implanted in the vicinity of each segmented section. The segmented sections are shown designated as pos(1), (2), and (3) from upstream along the channel for the cathode gas (oxygen or air). The matrix electrode other than the segmented sections, which represent an averaged performance over a whole cell, is called as pos(4). A circuit diagram for the segmented electrode separator is shown in Figure 2(b). Sections pos(1), (2), and (3), and matrix pos(4), are connected by a shunt circuit in series. The resistance values of the four parallel sections are regulated to be the same by adjusting the shunt resistance values ($R_1$, $R_2$, $R_3$ and $R_4$=97.06, 97.38, 96.53, 5.00 mΩ, respectively and $R_a$ is 1 mΩ). Sections pos(1), (2), and (3), and matrix pos(4), are connected in parallel to impose equal potential on all sections. The shunt resistance values were inversely proportional to the area of each electrode. An electronic load unit (PLZ164WA, Kikusui Electronics Corp.) was used for the resistance load.

## III. EXPERIMENTAL RESULTS

### A. Cell performance detected by segmented electrode

A segmented electrode detects local cell performance during power generation by using an electronic load unit (see Figure 2(b)).

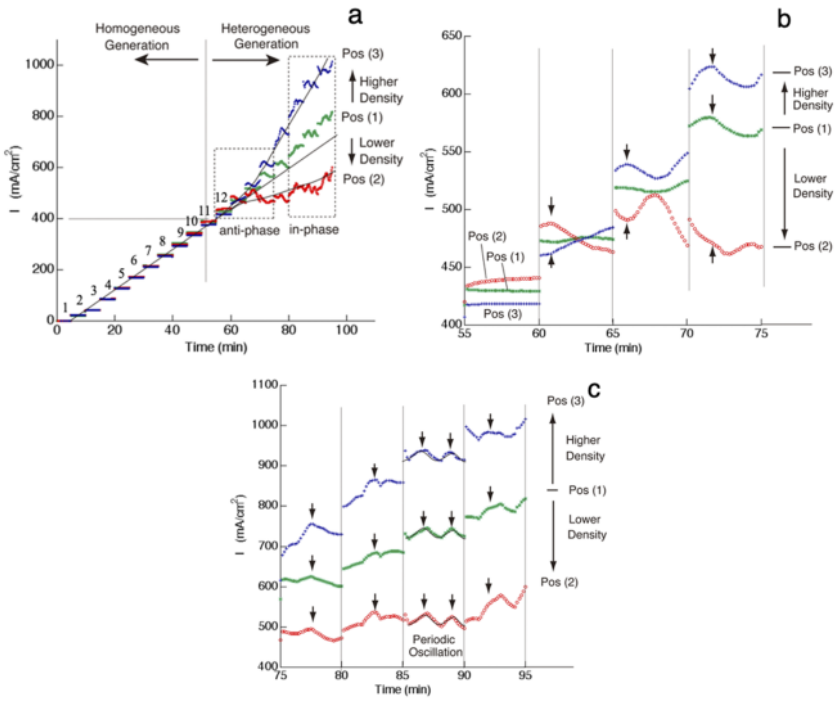


**FIG. 3.** (a) Plot of current density I (mA/cm$^2$) vs elapsed time (min) for different sections designated as pos(1), (2) and (3). Current density is increased with a step of 5 min. For the elapsed time (<55 min), three sections of pos(1), (2) and (3) exhibit same current density (homogeneous generation). For the elapsed time (>55 min), on the other hand, three sections exhibit different current densities (pos(3) shows higher and pos(2) shows lower) (heterogeneous generation) and start to oscillate with time in a way of anti-phase or in-phase. (b) Highlight of current density (mA/cm$^2$) at elapsed time from 55 to 75 min, obtained for segmented sections of pos(1), (2) and (3) (heterogeneous generation & anti-phase). (c) Highlight of current density (mA/cm$^2$) at elapsed time from 75 to 95 min, obtained for segmented sections of pos(1), (2) and (3) (heterogeneous generation & in-phase).

The load was applied stepwise and the time spent at each load was maintained for 10 min. Figure 3 shows the current for each section (pos (1), (2) and (3)) monitored over an elapsed time. Figure 3(a) shows the results over an entire time up to 95 min. In a time region shorter than 55 min, three different sections (pos (1), (2) and (3)) exhibit identical values; the current increases equally as the load increased, which is designated as ***homogeneous generation***. Meanwhile after 55 min, we found ***heterogeneous generation***. The current starts to heterogeneously distribute; the current at pos(2) (midstream) is lower and higher is at pos(3) (downstream), whereas pos(1) (upstream) keeps increasing of current with a same slope from before 55 min.

Figure 3(b) and (c) show close up views of the heterogeneous generation behavior, focusing on from 55 min to 75 min and from 75 to 95 min, respectively. In Figure 3(b), pos(2) first at 55min shows higher current density, which implies that chemical reaction producing water at cathode is more prominent compared to pos(1) and (3). Average current density considering pos(1), (2) and (3) is close to that at pos(1). From 60 to 65 min, the current density at pos(2) once increases and then starts to decreases. Corresponding to this change, the current density at pos(3) starts to increase (anti-phase synchronization). This suggests that flooding in a catalyst or GDL layer gradually occurred due to water formation in segmented section pos(2). Pos(1) shows stable current density during this period. The same behavior of anti-phase synchronization between pos(2) and (3) was observed in following two periods from 65 to 75 min. especially from 70 to 75 min, pos(1) starts to oscillate synchronized with pos(3).

In Figure 3(c) showing from 75 to 95 min, pos(2) also starts to be synchronized with pos(1) and (3) (in-phase synchronization). In the period from 85 to 90 min, the periodic oscillation was found for all positions, the periodic interval of which is about ~100 sec. We stress that heterogeneous generation and synchronization of current at each position should be due to two competitive factors at the cathode catalyst, (i) chemical reaction producing water and (ii) flooding prohibiting mass ($O_2$) transportation. Consequently, this rhythmic pattern is a non-linear phenomenon in an open & non-equilibrium system.

Figure 4(a) shows cell voltage obtained at pos(2) for < 400 mA/cm$^2$ (indicated as steps 2-12). At each step, we retained load for 5 min. Figure 4(b) shows cell voltage obtained for = 440 mA/cm$^2$. Cell voltage starts to oscillate with a time interval ~100 sec. It continues stably when the load is maintained at 440 mA/cm$^2$. When we increases the current higher (Figure 4(c)–(e)), the oscillation becomes more obvious, showing larger amplitude ΔV. This oscillation behavior in cell voltage is related to the oscillation in SANS intensity, which is shown later. This oscillation behavior is designated as a "***respiration***" mode of the fuel cell.

In Figure 5, so-called I-V curves (the potential measured at each position) are shown as a function of current density (*I*). The drop in the cell voltage accompanying an increase in current

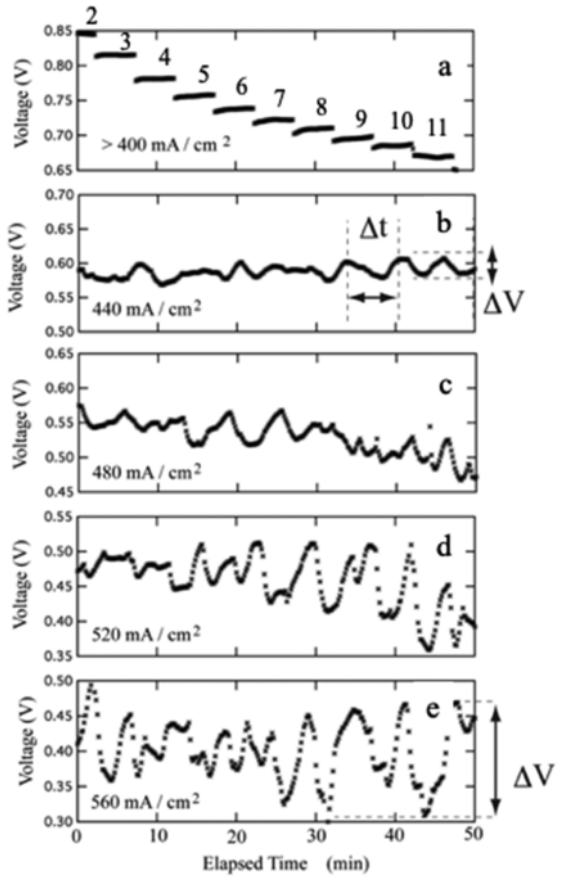


**FIG. 4.** Plot of cell voltage (V) vs elapsed time (min) for segmented section pos(2). (a) for I < 400 (mA/cm$^2$), (b) for I=440 (mA/cm$^2$), (c) for I=480 (mA/cm$^2$), (d) for I=520 (mA/cm$^2$)and (e) for I=560 (mA/cm$^2$), respectively. Amplitude of oscillation is ΔV.

density can be broken down into (a) activation loss of molecular oxygen at the cathode, (b) membrane resistance loss, and (c) oxygen concentration loss.

In the low current density region (<400 mA cm$^{-2}$), the I-V curve for section pos(4) and segmented sections pos(1)–(3) are approximately in agreement. This region is the resistance loss (b), in which the gradual decrease of the resistance value can be approximated as a constant. Meanwhile, in the high current density region (≥400 mA cm$^{-2}$), the voltage value of each section differs. The potential of the electrodes of pos(2) positioned midstream began to decrease first, simultaneously followed by that of the electrodes in pos(1), which was positioned upstream. This drop can be attributed to oxygen diffusion loss (c), because the resistance was approximately fixed during this period. In contrast, the electrodes in pos(3) positioned downstream maintained a generating state, keeping the voltage values expected by the resistance loss, until a high current density.

### B. Deuterium fuel cell; contrast variation using $D_2$ gas

During fuel cell operation, we switched fuel gas from hydrogen to deuterium and observed SANS. Figure 6 shows $q$-profiles of SANS obtained when using $H_2$ and $D_2$ gas. The scattering intensity at a scattering maximum $q_m$, due to inter-particle interference of water-clusters, significantly changes. The mean distance of water-clusters is given by $\Lambda$=5nm (=$2\pi/q_m$). For a case of $H_2$ gas, the intensity is larger, whereas for a case of $D_2$ gas, it is less. Note that the strong upturn of SANS appeared in the lower $q$-region is from catalyst or electrode layer.

According to the structural model,[7] the water-clusters are dispersed in a matrix of base polymer, i.e., polytetraflouoroethylene (PTFE). It was reported for the microstructure in a Nafion film that sulfonate groups are localized at the interface between water and PTFE. Therefore, the scattering contrast ($\Delta b_V$) to determine the intensity at $q_m$, is given approximately by the difference in coherent scattering length of PTFE and water. The coherent scattering length density of PTFE dominated by a fluorine atom is close to that of deuterium, whereas it is largely different from that for hydrogen. Consequently, the scattering contrast $\Delta b_V{}^2$ becomes larger when we use $H_2$ as compared to $D_2$.

Small-angle scattering $I(q)$ in a $q$-region around $q_m$ is attributed to the water-cluster network dispersed in PTFE $I_W(q)$, while $I(q)$ in the lower $q$ is due to crystalline domains in PTFE $I_C(q)$. $I(q)$ is given by

$$I(q) = I_C(q) + I_W(q). \quad (1)$$

We approximately reproduce $I_{cal}(q)$ as follows,

$$I_C(q) = I_C q^{-\alpha} \quad \text{with } \alpha = 1.97. \quad (2)$$

$I_W(q)$ is approximated by a Gaussian function, as follows,

$$I_{ion}(q) = I_m \exp[C(q - q_m)^2], \quad (3)$$

and

$$I_m = \Delta b_V^2 \Psi(1 - \Psi), \quad (4)$$

where $\Psi$ is volume fraction of space occupied by water cluster-network in the Nafion® film. The scattering contrast $\Delta b_V$, i.e., difference in coherent scattering length density, is rewritten by,

$$\Delta b_V = \phi b_{D_2O} + [1 - \phi] b_{H_2O} - b_{PTFE},$$

and therefore,

$$\Delta b_V = [b_{D_2O} - b_{H_2O}]\phi + [b_{H_2O} - b_{PTFE}] \quad (5)$$

where $\phi$ is water concentration of $D_2O$ in the ion channel. $b$ is coherent scattering. Note that $b_{PTFE}$, $b_{H2O}$ and $b_{D2O}$ are 4.75×10$^6$, -0.5×10$^6$ and 6.30×10$^6$ A$^{-2}$, respectively. As increasing the concentration of $D_2O$, the scattering intensity at $q_m$ monotonously decreases.

Next, we examined the time-evolution of SANS after changing fuel gas. By using time-resolved SANS, we investigated the intensity and $q$-position ($q_m$) as a function of time. Figure 7 shows intensity and $q$-position at the scattering maximum originating from the water-clusters. First, we operated a fuel cell with $H_2$ gas, and then at 250 sec, we switched hydrogen gas to $D_2$, and at 1500 sec again switched back to $H_2$ gas. The intensity at $q_m$ significantly changes

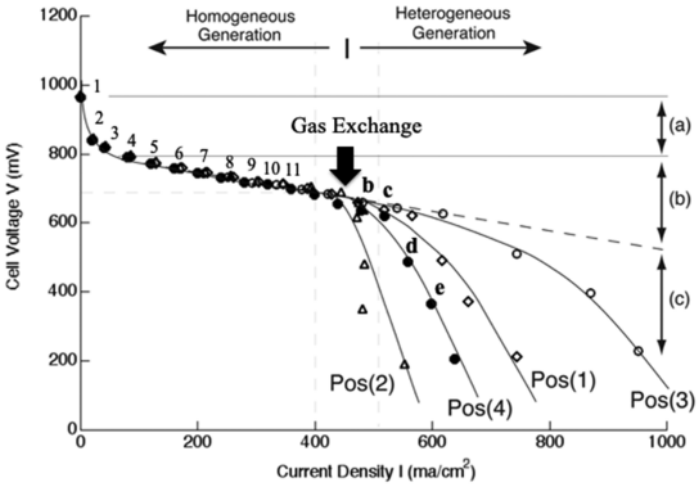


**FIG. 5**. I-V curves obtained from different sections from pos(1) to (4), corresponding to the operation shown in Figure 3 and 4. Each point is given by time-average of measured value. I-V curve shows (a) activation loss, (b) ohmic loss and (c) diffusion loss. Numbers (1-12) correspond to those in Figure 4(a). Diffusion loss starts in heterogeneous generation region (>400 mA/cm$^2$). Gas exchange experiment is performed at 440 mA/cm$^2$, indicated by thick arrow. Solid lines are a guide for eye.

as the fuel gas changes from $H_2$ to $D_2$ or from $D_2$ to $H_2$, which is synchronized with changing a type of hydrogen gas. The change in intensity is about 70%. Over a whole time, it should be denoted that the intensity at $q_m$ is oscillates around the mean value during periods until 250 sec or from 250 to 1500 sec. The concentration $\phi$ varying in time gives scattering length as a function of time ($\phi(t) \rightarrow b(t)$). $q_m$ also fluctuates in time during fuel cell operation at 440 mA/cm$^2$, which implies the water-cluster structure is swollen and de-swollen.

### C. Conventional contrast variation by mixing water

As a control experiment in order to determine $D_2O$ concentration in the Nafion® membrane during gas exchange operation, we performed conventional contrast variation experiments by preparing the mixed water ($H_2O/D_2O$). Nafion® films were immersed in the mixed water to exchange. Figure 8 shows SANS profiles obtained for the Nafion® swollen by the mixed water ($H_2O/D_2O$). As the $D_2O$ concentration increases, SANS intensity at the scattering maximum

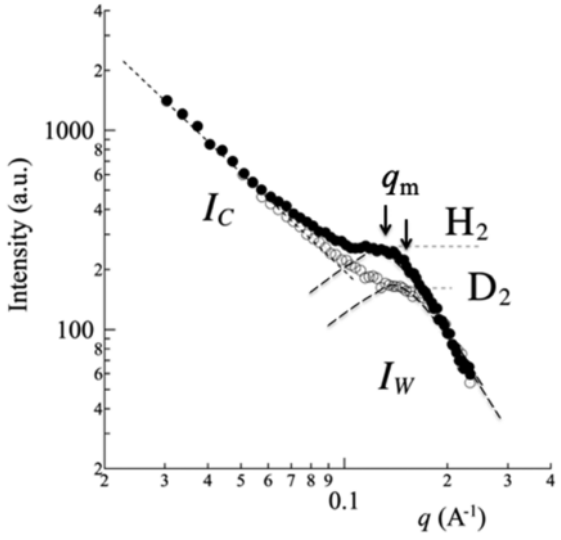


**FIG. 6**. SANS profile obtained for gas exchange $H_2$ and $D_2$, at I= 440 mA/cm$^2$ (black and white symbols are operation with $H_2$ and $D_2$ gas, respectively). $I_C$ and $I_W$ indicate scattering components from crystalline domain and water-cluster domains.

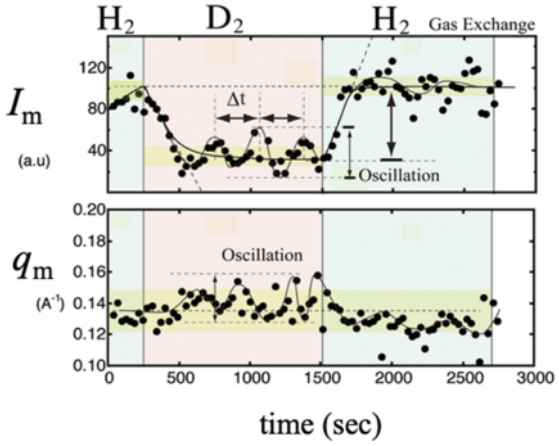


**FIG. 7**. SANS results of $I_m$ and $q_m$ as a function of time (sec). Anode gas was switched (i) $H_2 \rightarrow D_2$, and (ii) $H_2 \rightarrow D_2$, at 250 and 1500 sec, respectively. Oscillation behaviors in $I_m$ and $q_m$ (respiration mode) with time interval Δt are shown.

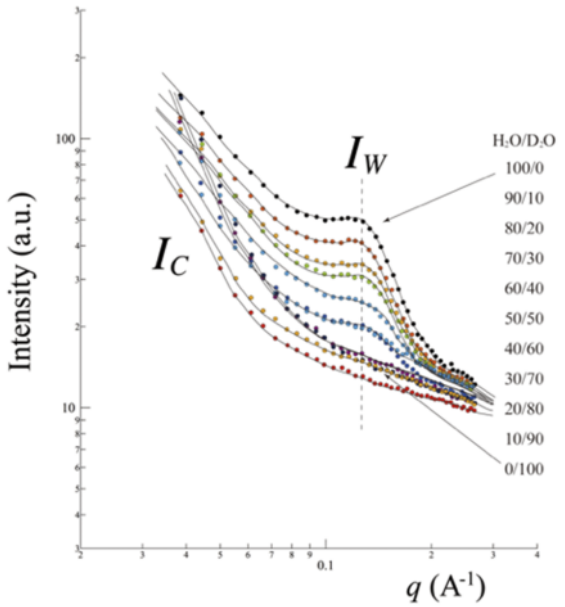


**FIG. 8.** SANS profiles obtained for Nafion® films immersed in mixed water ($H_2O/D_2O$) (conventional contrast variation). At low $q$, SANS originates from crystalline domain $I_C$, whereas at high q, SANS originates from water-cluster $I_W$. Solid lines are a guide for eye.

decreases. This is due to change in scattering contrast ($\Delta b^2$). Note that coherent scattering length of $D_2O$ is close to the base polymer of PTFE. We evaluated a ratio of the scattering intensity $R$; SANS intensity obtained at $q_m$ for ϕ normalized by that for ϕ=0,

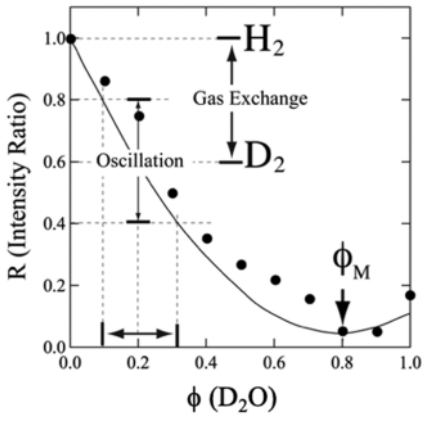


**FIG. 9.** Ratio of scattering intensity $I_m$ determined as a function of $D_2O$ concentration $\phi$. Minimum appears at $\phi_M$. Change by gas exchange and oscillation behaviors are indicated by double arrows. Solid line is a parabolic curve by eq. (7) with $\phi_M$=0.8.

$$R = I_{w,\phi}/I_{w,\phi=0} \tag{6}$$

Figure 9 exhibits the values of $R$, which is reproduced by a parabolic function of $\phi$ concentration of $D_2O$. Using eq. (5) and (6), $R$ is given by

$$R = \frac{\Delta b^2_{V,\phi}}{\Delta b^2_{V,\phi=0}} = \left(\frac{[b_{D_2O} - b_{H_2O}]}{[b_{H_2O} - b_{PTFE}]}\phi + 1\right)^2 \tag{7}$$

A contrast matching point $\phi_M$ is given by $R$=0,

$$\phi_M = [b_{PTFE} - b_{H_2O}]/[b_{D_2O} - b_{H_2O}]. \tag{8}$$

The solid line curve in Figure 9 is drawn by eq. (7) and the minimum intensity appears at $\phi_M$ = 0.8 (=5.25/6.5).

## IV. DISCUSSION

### A. Rhythmic oscillation of SANS at high current

First we summarize our results by SANS. In Figure 6, after switching $H_2$ gas to $D_2$ gas, it was found that SANS intensity at $q_m$ drops about 40%. From Figure 7, the amplitude of intensity fluctuation id about 20% of the mean value. The initial drop and oscillation are indicated in Figure 9. By carefully watching the result shown in Figure 7 and 9, the $D_2O$ (or deuteron) concentration in the Nafion® film is periodically oscillating at around a mean value of $\phi$=0.2 with amplitude $\Delta\phi$=∓0.1.

Next, we proceed our discussion according a scheme of flux balance in Ref. 1 (chapter 4.5 and 6.2). Total amount of deuterium in the Nafin® film $J_D$, which is attributed to $D^+$, HOD and $D_2O$, is determined by a balance between forward and back diffusion; total flux $J_D$ = forward diffusion $J_F$ + back diffusion $J_B$. The forward diffusion $J_F$ is decomposed into (i) deuteron flux by electron current $J_D$ and (ii) water flux by electro-osmotic drive $J_{EOD}$. Note that $J_D = \frac{j_e}{2F}$. According to Ref. 1, $J_{EOD}$ and $J_B$ are given by

$$J_{EOD} = \frac{j_e}{2F} 2n_d \frac{\lambda_w}{22} \text{ and } J_B = -\frac{\rho_{dry}}{M_m} D_\lambda \frac{d\lambda_w}{dZ} \tag{9}$$

where $\lambda_w$ is the number of water molecules around a $SO_3$ group, $D_\lambda$ is a diffusion coefficient of water in the membrane, $\rho_{dry}$ is the mass density of membrane at a dried state and $M_m$ is molecular weight of the membrane.

The charge transport via proton strongly coupled with water forming hydronium ion ($H_3O^+$) in the membrane. Proton diffuses in the membrane and drags water molecules (electro-osmotic drag). We define an electro-osmotic drive coefficient $n_d$ as the number of water molecules accompanying the movement of each proton, $n_d$=$n_{H2O}/n_P$.

$j_e$ is related to a reaction rate $R_C$ according to $j_e = 2R_C$. As a result, we obtain

$$J_D = \frac{2R_C}{2F}\left[1 + 2n_d\frac{\lambda_w}{22}\right] - \frac{\rho_{dry}}{M_m} D_\lambda \frac{d\lambda_w}{dZ} \tag{10}$$

The first term of forward diffusion of proton (from anode to cathode), which is proportional to the current $j_e$ and reaction rate RC. The second term of back diffusion is proportional to ($d\lambda_w/dZ$); heterogeneous water distribution along a film thickness (z-axis).

When the reaction proceeds enough, the second term of back diffusion becomes dominant. When the membrane is not fully swollen, the first and second terms are balanced. Flooding at the

cathode (catalyst or GDL) does not occur. This is the case of I< 400 mA/cm$^2$, we studied. On the other hand, for operation at higher current density, when swelling of membrane starts to be saturated ($d\lambda_w/dZ = 0$). Flooding at the cathode catalyst starts to occur causing oxygen diffusion loss. Consequently, the reaction is decelerated, which might be a physical reason for a respiration mode.

$R_C$ is a reaction rate at the cathode, which is given by as follows,

$$R_C = [H^+]^2[O_2]_{app}, \tag{11}$$

where $[H^+]$ and $[O_2]_{app}$ are concentration of proton and $O_2$ gas.

If water production at high current density proceeds more than water excretion from a gas flow channel, flooding occurs in the electrode of MEA. Flooding affects mass transportation of oxygen gas at the surface of Pt particle, which we formulize as follows,

$$[O_2]_{app} = [O_2] - k[H_2O]^l, \tag{12}$$

where parameters $k$ and $l$ changing in time control $O_2$ concentration at the Pt surface. The second term in eq. (12), related to flooding, decelerates a chemical reaction. Thus, flooding is a feedback to slowing down of chemical reaction and the rhythmic oscillation in current and small-angle scattering in terms of $q_m$ and intensity. The intensity of SANS is proportional to $\Delta b_V{}^2$, which is composed of $\phi(t)$ (concentration of $D_2O$). The relation between $J_P$ and $\phi(t)$ is given by

$$\phi = C \int_{t_1}^{t_2} J_D dt \tag{13}$$

where $C$ is a normalization factor.

Therefore, the scattering contrast in eq. (5) is rewritten as,

$$\Delta b_V = K_1 \int_{t_1}^{t_2} J_P dt + K_2$$

$$\text{With } K_1 = C[b_{D_2O} - b_{H_2O}] \text{ and } K_2 = [b_{H_2O} - b_{PTFE}] \tag{14}$$

We denote that $\Delta t$ (= $t_1$- $t_2$) is order of 100sec. During a stationary operation with supplying $D_2$ gas, the scattering intensity at $q_m$ and $q_m$ rhythmically oscillate with a time interval is about 100 sec (a ***respiration*** mode). This results from a counter balance between (i) back diffuse of generated $D_2O$ from the cathode to the electrolyte, and swelling by $H_2O$ supplied as humidity.

### B. Synchronization in lateral direction

According to the results obtained by NR (Refs. 3 and 4), the flooding starts to appear as the load is increased. As increasing current density to about 240 mA/cm$^2$, first water appears at the upper part of fuel cell (part of fuel cell), which is close to the air inlet (see Figure 10). Then at 400 mA/cm$^2$ water appears widely in a plane of fuel cell extending toward the bottom. Note that we employed a *counter-flow* condition where hydrogen is supplied along a serpentine gas flow channel from bottom and air from the top. At 640 mA/cm$^2$, the flooding detected by NR appears homogeneously in the lateral direction (from the inlet to outlet of $H_2$ gas).

In Refs. 3–5, SANS was obtained in $q$-region around $q_m$ during operation by changing current density from 0 to 640 mA/cm$^2$. As the current density increased, the $q$-position of this peak shifts lower $q$, and its intensity increases, which indicates that the water-cluster becomes larger due to swelling with produced water. From $q_m$, we evaluated a mean distance of water clusters $L_W$ (=$2\pi/q_m$) as a function of current density. At 400 mA/cm$^2$, $L_W$ increases first at upstream from about 40 nm to 44 nm (10% increase). Next $L_W$ at the midstream (center of fuel cell) reaches to the maximum value 44nm. $L_W$ at the bottom swelling does not changes during operation at lower current density, however, finally at higher current density about 640 mA/cm$^2$, $L_W$ at the bottom stream reaches to 44nm.

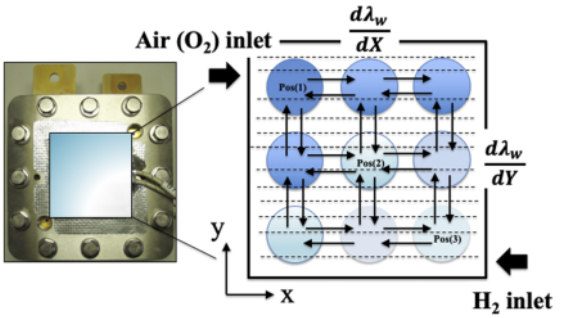


**FIG. 10.** Schematic diagram of heterogeneous water distribution in PEM during operation ($\frac{d\lambda_w}{dX}$ and $\frac{d\lambda_w}{dY}$) and synchronization along lateral direction in (x, y) plane.

Figure 10 schematically shows synchronization in a lateral direction ($X$, $Y$) in a membrane. Lateral heterogeneity in $\lambda_w$, causes a non-zero gradient ($\frac{d\lambda_w}{dX}$ and $\frac{d\lambda_w}{dY}$). In the current density region below 440 mA/cm$^2$, $\frac{d\lambda_w}{dX}$ and $\frac{d\lambda_w}{dY}$ should be negligibly small. However, at 400 mA/cm$^2$, $\frac{d\lambda_w}{dX}$ and $\frac{d\lambda_w}{dY}$ might be negligible (see Figure 10). At the current density close to 640 mA/cm$^2$, $\frac{d\lambda_w}{dX}$ and $\frac{d\lambda_w}{dY}$ become small (homogenous water distribution). Due to the heterogeneity of $\lambda_w$ in a lateral direction ($X$, $Y$), the synchronization of cell performance occurs.

## V. CONCLUSION

Using time-resolved SANS and segmented electrode, we observed the heterogeneous performance, which is referred as a ***respiration*** mode of fuel cell. Neutron is a marvelous probe to see a function system of fuel cell under operation. The observation profits to explore a boundary between material and living things.

## APPENDIX A: DEUTERIUM FUEL CELL

The cell performance when using $D_2$ gas (*deuterium fuel cell*) was examined by operating a fuel cell with three different conditions of (i) $D_2$ gas humidified with $D_2O$, (ii) $D_2$ gas humidified with $H_2O$ and (iii) $H_2$ gas humidified with $H_2O$. Figure 11 shows so-called I-V curves, in which $V_c$ is shown as a function of $I_m$. Higher cell performance was achieved with a condition (i), as compared to the cases of (ii) and (iii). The difference in voltage is about 30mV higher at the current density between 100 and 250 mA/cm$^2$ in a current density region of ohmic loss. According to the reference, Gibbs free energy for $D_2$ in a liquid state is slightly larger than that for $H_2$ ($\Delta G$=6 KJ/*mol*). We estimate a cell voltage $\Delta V_c$ using $\Delta G$=6 KJ/*mol*

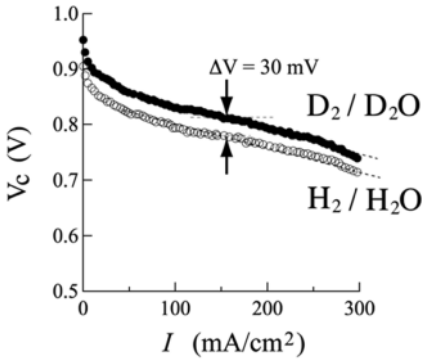


**FIG. 11.** I-V curves obtained by operations with hydrogen gas ($H_2$) humidified by $H_2O$ and deuterium ($D_2$) gas humidified by $D_2O$ (open and filled circles, respectively) as a function of current density ($I$). The difference in cell voltage between two curves is $\Delta V$=30 mV for from 0 to 300 mA/cm$^2$.

and a Faraday's law

$$\Delta V_c = \Delta G/(2F), \tag{A1}$$

where $F$ is a faraday constant ($F$ = 96500 C/mol). We obtained $\Delta V_c$=30mV, which is identical with the value detected by our experiment.

The case of $D_2$ gas humidified by $H_2O$ was examined for a Nafion® membrane coated (a) with and (b) without catalyst (carbon-supported Pt). For the case (a) with a catalyst, the water is composed of $H_2O$, $D_2O$ and HOD. This result indicates that at the anode catalyst, deuteron $D^+$ is separated from $D_2$ gas and exchanged with H in $H_2O$. For the case (b) without a catalyst, the water collected at cathode is composed of pure $H_2O$. It implies that $D_2$ gas stably exist without exchanging hydrogen in water. For the case (a) $D_2$ gas humidified by $H_2O$ and with a catalyst, the excess free energy $\Delta G$ (=6 KJ/*mol*) is released so that $V_c$ for the case (ii) becomes same with that for the case (iii).

## APPENDIX B: MIXED WATER OF $H_2O/D_2O$

A mixing behavior of $H_2O$ and $D_2O$ was examined by IR spectroscopy. Figure 12(a) shows IR spectra obtained for mixtures of $H_2O$ and $D_2O$. Immediately after mixing, we recognize spectrum maxima originating from HDO in addition to those for $H_2O$ and $D_2O$. The intensity of IR spectra is proportional to concentration of each component. Relative ratios of peak intensity are shown in Figure 12(b). If we denote a volume fraction of HDO as $\phi_{HDO}(t)$, volume fractions of $D_2O$ and $H_2O$ are given by $[\phi_{D2O}(t)$-$\phi_{HDO}(t)]$ and $[1$-$\phi_{D2O}(t)$-$\phi_{HDO}(t)]$. Then $\Delta b_V$ is re-written as follows,

$$\begin{aligned}\Delta b_V &= [\phi_{D2O}(t) - \phi_{HDO}(t)]\, b_{D2O} + [1 - \phi_{D2O}(t) - \phi_{HDO}(t)]\, b_{H2O} \\ &\quad + 2\phi_{HDO}(t)\, b_{HDO} - b_{PTFE} \\ &= \phi_{D2O}(t)\, b_{D2O} + [1 - \phi_{D2O}(t)]\, b_{H2O} \\ &\quad + \phi_{HDO}(t)\, [2b_{HDO} - b_{D2O} - b_{H2O}] - b_{PTFE}\end{aligned} \tag{A2}$$

After averaging over length scales longer than a molecular size of water, a term of $[2b_{HDO}$-$b_{D2O}$-$b_{H2O}]$ in eq. (6) becomes equal to zero, so that eq. (A2) is identical to eq. (5)

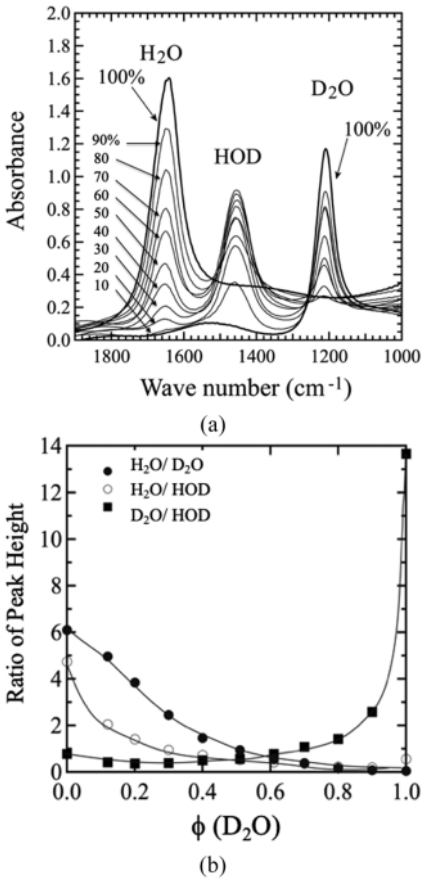


**FIG. 12.** (a) IR spectra obtained for mixed water ($H_2O/D_2O$). (b) Ratio of peak heights of IR.

## REFERENCES

[1]R. O'Hayre, S. Cha, W. Colella, and F. B. Prinz, *Fuel Cell Fundamentals* (John Wiley & Sons, NY, 2006).
[2]P. Mitchell, Nature. **191**(4784), 144–148 (1961).
[3]H. Iwase, S. Koizumi, H. Iikura, M. Matsubayashi, D. Yamaguchi, Y. Maekawa, and T. Hashimoto, Nucl. Inst. And Meth. A **605**, 95–98 (2009).
[4]A. Putra, H. Iwase, D. Yamaguchi, S. Koizumi, Y. Maekawa, M. Matsubayashi, and T. Hashimoto, J. Phys. Conf. Ser. **247**, 012044 (2010).
[5]S. Ueda, S. Koizumi, and Y. Tsutsumi, Results in Physics **12**, 504–511 (2019).
[6]S. Ueda, S. Koizumi, and Y. Tsutsumi, Results in Physics **12**, 1871–1879 (2019).
[7]T. D. Gierke, G. E. Munn, and F. C. Wilson, J. Polym. Sci., Polym. Phys. **19**, 1687–1704 (1981); W. Y. Hsu and T. D. Gierke, J. Membr. Sci. **13**, 307–326 (1983).
[8]S. Koizumi, H. Iwase, J. Suzuki, T. Oku, R. Motokawa, H. Sasao, H. Tanaka, D. Yamaguchi, H. M. Shimizu, and T. Hashimoto, J. Appl. Cryst. **40**, s474–s479 (2007).

# Heterogeneous cell performance of polymer electrolyte fuel cell at high current operation: Respiration mode as non-equilibrium phenomenon

ORIGINALITY REPORT

| 12% | 7% | 9% | 3% |
|---|---|---|---|
| SIMILARITY INDEX | INTERNET SOURCES | PUBLICATIONS | STUDENT PAPERS |

MATCH ALL SOURCES (ONLY SELECTED SOURCE PRINTED)

2%

★ link.springer.com

Internet Source

| | | | |
|---|---|---|---|
| Exclude quotes | Off | Exclude matches | Off |
| Exclude bibliography | Off | | |